Available online at www.sciencedirect.com

SciVerse ScienceDirect

Ceramics International 39 (2013) 6107–6112

CERAMICS INTERNATIONAL

www.elsevier.com/locate/ceramint

Crystallization behavior and microstructure of ErF_3 nanocrystals in an oxyfluoride glass

Amit Mallik[a], Biswajit Pal[b], Paritosh Kundu[a], Arunabha Basumajumdar[a,*]

[a]Department of Chemical Technology, University of Calcutta, 92A. P.C. Road, Kolkata 700009, India
[b]Department of Chemistry, St. Paul's C.M. College, University of Calcutta, 33/1, Raja Rammohan Roy Sarani, Kolkata 700009, India

Received 30 November 2012; received in revised form 10 January 2013; accepted 10 January 2013
Available online 20 January 2013

Abstract

Nanocrystallization of ErF_3 in oxyfluoride glass of composition $55SiO_2 \cdot 20Al_2O_3 \cdot 15Na_2O \cdot 10ErF_3$ (mol%) has been observed by its heat treatment above the glass transition temperature. The crystallization mechanism of this glass has been substantiated by the microstructural and compositional changes in the crystalline phase. Studies have been made through dilatometry, X-ray diffraction (XRD), transmission electron microscopy (TEM) and differential scanning calorimetry (DSC). Maximum crystal size of 20 nm has been obtained, on variation of heat treatment time and temperature. Transmission electron microscopy (TEM) images of the as-annealed glass before heat treatment showed nonoccurrence of phase separation on quenching the melt. But after heat treatment for 10 h at 620 °C, ordered regions of dark contrast (0.5 nm) with respect to the matrix had appeared. These regions are believed to be associated with the process of onset of nucleation of fluorite phase.

Keywords: Oxyfluoride glass; Annealed glass; Crystallization mechanism; Microstructure-final

1. Introduction

Rare earth doped oxyfluoride glass ceramic systems comprise mainly oxide glasses and can offer optical properties of rare earth fluoride crystals [1]. These glasses combine the mechanical strength and chemical resistance of aluminosilicate glasses with low phonon energy and facilitate incorporation of rare earth ions in the fluoride crystals. Erbium fluoride glass ceramics are excellent materials for photonic applications [2–5] due to their ability to host rare-earth ions in crystalline precipitates in which the phonon energy is very low. If the optically active ion is incorporated into the fluoride crystalline phase, the intensity of the characteristic laser emission is enhanced. Ideally the crystal size should be in the range 5–100 nm, with a narrow size distribution in order to minimize scattering losses [6,7]. The crystallization of fluoride phase is achieved by heat treatment at temperatures slightly above the glass transition temperature (T_g). Base glass composition, temperature and time of heat treatment will influence the crystallization process, phase composition and crystal size.

Chen et al. [8] studied a complete spectroscope of energy transfer processes in oxyfluoride glass ceramics containing CaF_2 nano-crystals doped with various amounts of Er^{3+} and Yb^{3+}. The coefficients of energy transfer from Er^{3+} to Yb^{3+} and transfer from Yb^{3+} to Er^{3+} back for the glass ceramic system were determined to be 5.8×10^{-16} and 1.3×10^{-16} cm^3/s, respectively.

Pan et al. [9] studied the upconversion luminescence for Er^{3+} in a germanate–oxyfluoride and a tellurium–germanate–oxyfluoride transparent glass–ceramic using 800 nm excitation and observed significant increase in upconversion luminescence of transparent glass–ceramics in comparison to those of corresponding as-prepared glasses.

Gugov et al. [10] observed that the transparent glass ceramics in the system $SiO_2 \cdot B_2O_3 \cdot PbO \cdot CdO \cdot PbF_2 \cdot CdF_2 \cdot YbF_3 \cdot ErF_3$ showed infrared to visible anti-Stokes (upconversion) luminescence. Both the Stokes and anti-Stokes luminescence spectra of glasses could be explained

*Corresponding author. Tel.: +91 33 2351 9755; fax: +91 9433459595.
E-mail address: a.basumajumdar@gmail.com (A. Basumajumdar).

0272-8842/$ - see front matter © 2013 Published by Elsevier Ltd and Techna Group S.r.l.
http://dx.doi.org/10.1016/j.ceramint.2013.01.028

with clustering of the Yb^{3+} and Er^{3+} ions in fluorine-rich regions. At the annealing temperature these regions act as nucleation precursors.

Zeng et al. [11] studied Er^{3+} doped transparent oxyfluoride glass ceramics, obtained by heat treatment of the precursor glasses with compositions $50SiO_2 \cdot xPbF_2 \cdot (50-x)PbO \cdot 0.5ErF_3$ in (mol%). The intensity of upconversion of luminescence significantly increased in glass ceramics compared to that of precursor glass. The emission bands, centered on 660 nm and 410 nm, were simultaneously observed in glass ceramics but could not be seen in the precursor glass.

In the present work, the process of crystallization of oxyfluoride glass and its crystallization kinetics, have been analyzed using dilatometry, DSC, XRD, and TEM.

2. Experimental

2.1. Glass synthesis, crystallization and chemical analysis

The glass-forming compositions studied are represented by the generic formula:

$55SiO_2 \cdot 20Al_2O_3 \cdot 15Na_2O \cdot 10ErF_3$.

Glass batches having above mol% compositions were prepared from SiO_2, Al_2O_3, Na_2CO_3, Al_2O_3 and ErF_3 raw materials. Batches were at first calcined for 2 h at 1200 °C and then melted for 1.5 h at 1550 °C. The molten batches were quenched and remelted twice in order to achieve the homogeneous transparent glasses. Glass–ceramics were obtained by controlled crystallization of ErF_3 at heat treatment temperatures between T_g+30 °C for various duration of time.

The above glass samples were analyzed by X-ray Fluorescence Spectroscopy (XRF) with a Panalytical Spectrometer (Epsilon 5). The contents of these oxides were determined by employing the melting method with $Li_2B_4O_7$. The fluorine content was analyzed with hard-pressed pellets of powdered glass (~6 g) in order to avoid volatilization. The batch composition and melted composition of the oxyfluoride glasses are presented in Table 1. The loss of fluorine during the melting process in air is approximately 38%, which is similar to the observation made by Pablos-Martin et al. [12].

Table 1
Batch composition and melted composition compositions (in mol%) of base glass.

Glass components	**Batch composition** (mol%)	**Melted composition** (mol%)
Na_2O	15.0	14.8
Al_2O_3	20.0	20.5
SiO_2	55.0	55.1
ErF_3	10.0	6.2
Er_2O_3	0.0	3.2
F^- (wt%)	6.5	4.2

2.2. Characterization techniques

2.2.1. X-ray diffraction

Crystal phase analysis of glass–ceramics was carried out after heat treatment at 620 °C for different duration of time. The ceramised glass samples were ground to ~75 μm. XRD experiments were performed by X-ray powder diffractometer (PW 1830, Panalytical) using Ni filtered Cu-k_α, X-radiation with scanning speed of 0.05°(2θ) per minute. The diffraction pattern was recorded within Bragg's angle ranges $10° < 2\theta < 70°$. The phases were identified by JCPDS numbers (ICDD—PDF2 data base).

2.2.2. Transmission electron microscopy

Glass–ceramic samples were ground to a thickness of < 100 μm using SiC paper ending with 1200 grit for TEM (Transmission Electron Microscopy) measurements. An epoxy adhesive was used to mount a copper support ring of diameter 3 mm and 1 mm hole was performed on the thinned sample. The samples were thinned by operating the Gatan Dual Ion Beam Miller, at an incident angle of 15°, with an accelerating voltage of 6 kV and a combined gun current of 6 mA. Samples were carbon coated and analyzed by TEM (JEOL JEM 3010 No. EMI 130005-8 at 300 kV) by an ultra-thin window.

2.2.3. Differential scanning calorimetry

The Differential Scanning Calorimetry (DSC) measurements were performed using Setaram Instrument (Model Setsys Evolution 16/18) with powdered Al_2O_3 as inert reference material. In this work, non-isothermal experiments were performed with finely powdered glass samples (~ 200 μm) of about ~100 mg with particle size of 1–1.20 mm in order to reproduce bulk conditions. The DSC scans were carried out at different heating rates (5, 10, 15, 20, 30, 40 °C/min).

Analytical models of Kissinger and Marrota were used to analyze the DSC data and to determine the activation energy for crystallization. Avrami exponent was also calculated by Augis-Bennet equation.

3. Results and discussion

3.1. X-ray diffraction and the crystallization process

The X-ray diffraction patterns of the glass–ceramic samples after heat treatments at 620 °C for varying times between 1 and 80 h are shown in Fig. 1. The JCPDS reference files have been used to identify the crystal phase. The orthorhombic erbium fluoride (PDF file no. 00-005-0541) is observed as major phase. Crystal phase of erbium fluoride was identified after 1 h of heat treatment at 620 °C. The peak intensity of erbium fluoride increases with increase in heat treatment time. The crystallite size of the erbium fluoride was calculated from the (111) peak of ErF_3 ($2\theta \approx 27.9°$) using the Scherrer

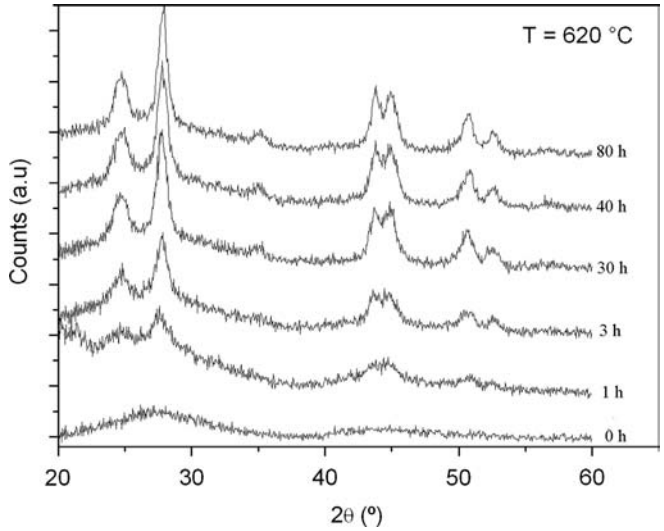

Fig. 1. XRD patterns of glass samples treated at 620 °C for a duration of 0, 1, 3, 30, 40 and 80 h.

formula [13].

$$D = \frac{K\lambda}{\beta \cos\theta}$$

where D is the crystallite size, k is a shape factor whose value is 0.9 [12], λ is X-ray wavelength, β is the full width at half maximum of the peak and θ is the Bragg angle. The result showed that at 620 °C, crystallites grew in size ranging from 10 to 20 nm.

3.2. TEM characterization

Transmission electron micrographs of the as-annealed glass showed a uniform field with no visible scattering (Fig. 2).

However, after heat treatment for 10 h at 620 °C, ordered regions of dark contrast of 0.5 nm diameter embedded in glass matrix is shown in Fig. 3. Based on dark contrast with respect to the matrix and evidence of ordering, it is suggested that they are associated with separation of liquid droplets.

But, after heat treatment for 40 h at 620 °C, the liquid–liquid phase separation of droplets enriched in elements of high atomic number is shown in Fig. 4. The droplets are amorphous with an average diameter in the range between 15 and 35 nm.

After heat treatment for 80 h at 620 °C, the average size of the phase separated droplets did not change significantly (Fig. 5). The shape of the phase-separated droplets (ErF_3 crystallites) became less spherical, which is corroborated by the XRD results presented in Section 3.1.

TEM and EDX analyses [14] indicate that the phase-separated droplets contain not only erbium and fluorine but also silicon and oxygen, in addition to traces of aluminum. It may be observed, that on annealing, the growth of the ErF_3 crystallites contained in the droplets, is limited slightly by excess of silicon. After completion of the crystallization process, several ErF_3 nanocrystals (9 nm diameter) are formed.

Fig. 2. Transmission electron micrograph of as-annealed glass-sample.

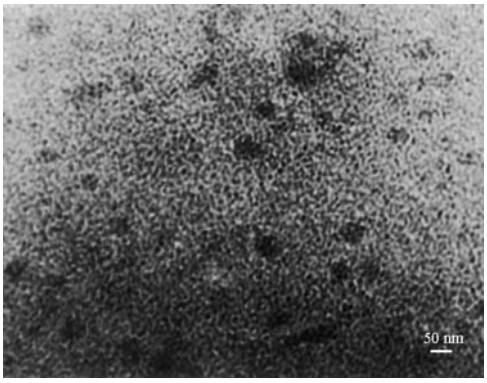

Fig. 3. Transmission electron micrograph of glass–ceramic sample heated at 620 °C for 10 h.

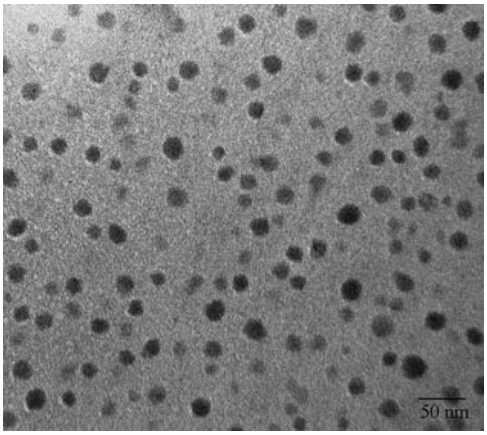

Fig. 4. Transmission electron micrograph of glass–ceramic sample heated at 620 °C for 40 h.

3.3. DSC analysis and crystallization kinetics

DSC curves for glass samples at a heating rate of 5, 10, 15, 20, 35 and 40 °C/min are shown in Fig. 6. The glass transition temperature (T_g) is determined from the point of intersection of two tangents drawn on the lines leading to depression in the baseline of the curves. Crystallization

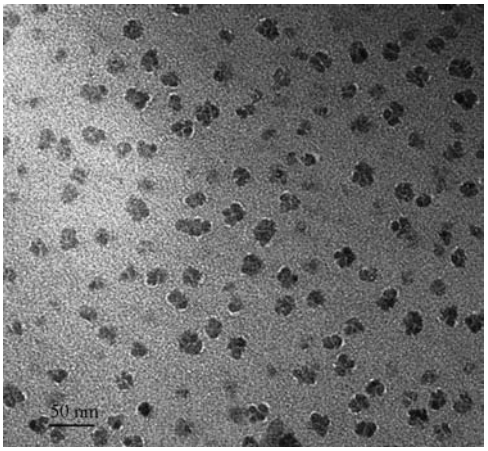

Fig. 5. Transmission electron micrograph of glass–ceramic sample heated at 620 °C for 80 h.

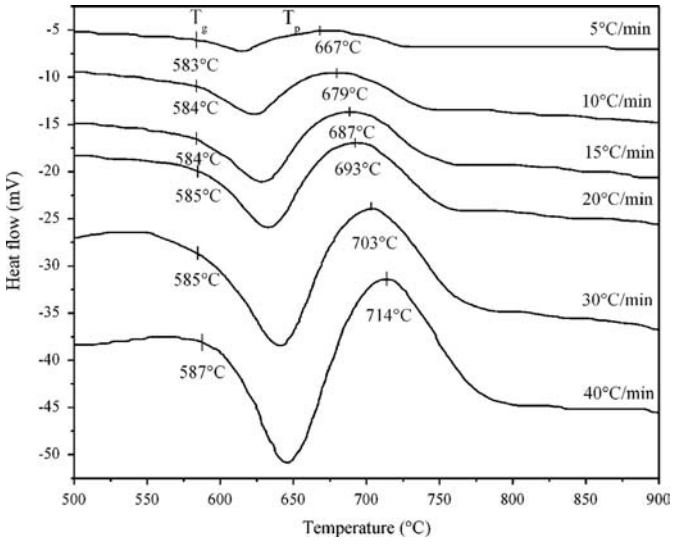

Fig. 6. Differential Scanning Calorimetry curves of the glass recorded from 5 to 40 °C/min.

peak temperature (T_p) corresponds to ErF3 crystallization. The glass transition temperature of the oxyfluoride glass was 585 ± 2 °C. The variation of the glass transition temperature is a function of the heat treatment time at 620 °C. It was observed that glass transition temperature of the glass heated at 620 °C for 20 h had increased by 60 °C compared to as-annealed glass and remained almost same even after heat treatment for longer durations. Increase of initial glass transition temperature (T_g) may be described by the reduction of fluoride ions in the glass matrix due to the crystallization of ErF_3, resulting in an enhancement of network forming ions in the residual glass matrix, which leads to an increase in glass transition temperature (T_g). Consequently, the change in glass transition temperature is insignificant even after heat treatment with durations longer than 20 h.

The isothermal kinetics of glass crystallization is studied on the basis of the Johnson–Mehl–Avrami (JMA) equation [15–21].

$$x = 1-\exp[-(kt)^n] \quad (1)$$

where x is the volume fraction crystallized at a given temperature during time t; k is the reaction rate constant and n is the Avrami exponent, which is a dimensionless factor depending on the nucleation process and growth morphology.

Based on Johnson–Mehl–Avrami equation, non-isothermal crystallization kinetics of glass can be described by the Kissinger and Ozawa equations [22–25].The Kissinger equation:

$$\ln\frac{T_p^2}{\beta} = \frac{E}{RT_p} + C \quad (2)$$

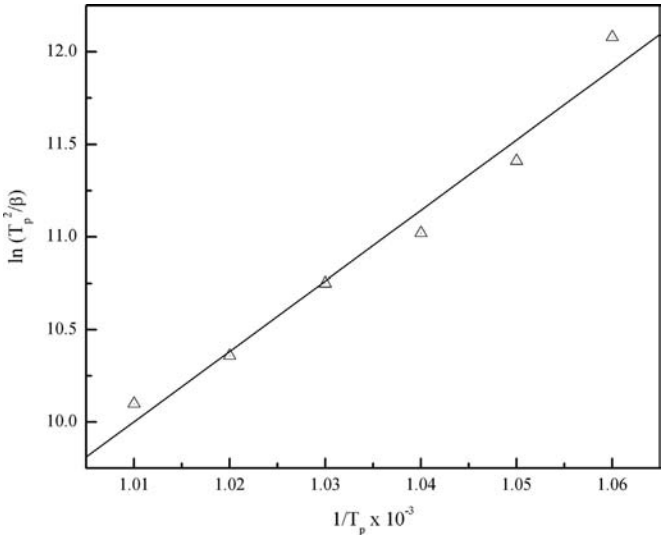

Fig. 7. The Kissinger plot of $\ln(T_P^2/\beta)$ against $1/T$p at crystallization peak temperature (Tp).

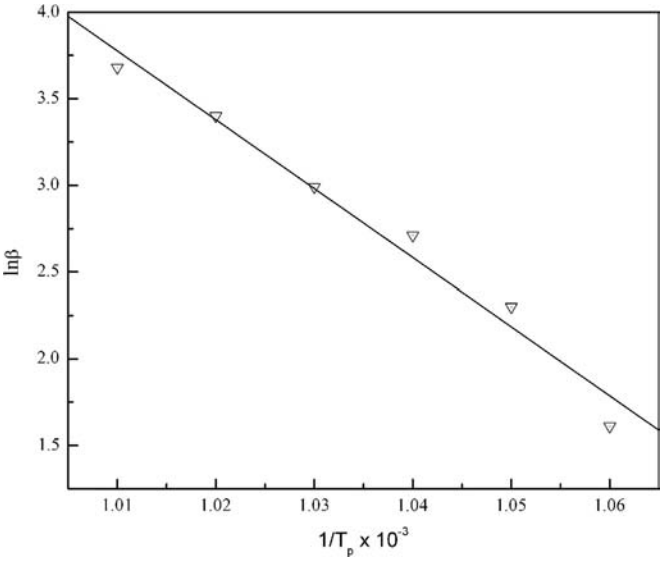

Fig. 8. The Ozawa plot of $\ln\beta$ against $1/T$p at crystallization peak temperature (Tp).

Table 2
Values of activation energy (Kissinger equation [E_K] + Ozawa equation [E_O]) and Avrami exponent.

Heating rate (β) (°C/min)	Crystallization peak temperature T_p (K)	Activation energy (E) (KJ/mol)		Average activation energy (E) (KJ/mol)	Avrami exponent (n)	Average Avrami exponent (n)
		Kissinger (E_k)	Ozawa (E_o)			
5	940	316.4	330.8	323.6	1.13	0.905 ≈ 1.00
10	952				1.05	
15	960				0.90	
20	966				0.85	
30	976				0.80	
40	987				0.70	

The Ozawa equation:

$$\ln\beta = -\frac{E}{RT_p} + C \quad (3)$$

where T_p is the crystallization peak temperature in a DTA curve, β is the heating rate, E is the activation energy of crystal growth, R is the universal gas constant and C is constant.

Using the Kissinger equation (2), $\ln(T_p^2/\beta)$ was plotted against $1/T_p$ and the slope of the plot is equal to E/R (Fig. 7), from which E can be calculated. Similarly using the Ozawa equation (3), $\ln\beta$ was plotted against $1/T_p$ and the slope of the plot is equal to $-E/R$ (Fig. 8), from which E can be calculated. The values of activation energy are given in Table 2.

From the Augis–Bennett equation [26], the value of Avrami exponent (n) can be estimated using the value of activation energy

$$n = \frac{2.5}{\Delta T} \times \frac{RT_p^2}{E} \quad (4)$$

where, n is the Avrami exponent or crystallization index and ΔT is the full width of the exothermic peak at half-maximum intensity. The values of Avrami exponent are given in Table 2. The crystallization index (n) depends upon the actual nucleation and growth mechanism. According to the JMA theory, crystallization index (n) depends on the crystallization manner, where $n \cong 1$ indicates that the bulk crystallization, $n \cong 2$ means that the surface crystallization dominates overall crystallization, $n \cong 3$ means that the two dimensional crystallization or volumetric crystallization, $n \cong 4$ means that the three dimensional crystallization for bulk materials mechanism [27–30].

In the present study the value of Avrami exponent (n) is determined using Eq. (4), n is close to 1, which indicates that the bulk crystallization mechanism with a constant number of nuclei.

4. Conclusion

1. Glass transition temperature (T_g) increased with heat treatment time at 620 °C, indicating enhancement in network formers in the glassy matrix and consequent fluorine crystallization. The narrow variation of crystal size on heat treatment from 1 to 80 h at 620, 660 and 680 °C indicated a low crystal growth velocity.
2. TEM analysis indicated the absence of crystallization in the as-annealed glass.
3. TEM analysis showed that after heat treatment for 10 h at 620 °C, ordered structures of about 0.5 nm diameter have grown, which is the first step in the development of nucleation of the fluorite structured crystalline phase.
4. Calculation of Avrami parameter/exponent (n) from DSC data, indicated bulk crystallization from a well-nucleated sample via a two-dimensional growth mechanism (nanoplates) of nuclei in the base glass. Besides above, DSC curves performed at different nucleation temperatures showed that crystallization takes place from the preexisting active sites.
5. The broadened profiles of certain reflections in the XRD data of the glass–ceramics provided supporting evidence for the growth of nanoplate-shaped crystals.

Acknowledgments

Financial support from the University Grant Commissions (UGC), under major research project is gratefully acknowledged. SEM and XRD facilities have been provided by the Technical education quality improvement program (TEQIP). One of the authors, AM thanks University Grant Commission (UGC), New Delhi, India, for providing Junior Research Fellowship (UGC-RGNF).

References

[1] F. Auzel, D. Pecile, D. Morin, Rare earth doped vitroceramics: new, efficient, blue and green emitting materials for infrared up-conversion, Journal of the Electrochemical Society 122 (1975) 101–107.
[2] D.C. Tran, G.H. Sigel, B. Bendow, Heavy metal fluoride glasses and fibers: a review, Journal of Lightwave Technology 2 (5) (1984) 566–586.
[3] B.J. Ainslie, S.T. Davey, D. Szebesta, J.R. Williams, M.W. Moore, T. Whitley, R. Wyatt, A review of fluoride fibres for optical amplification, Journal of Non-Crystalline Solids 184 (1995) 225–228.

[4] M. Yamada, T. Kanamori, Y. Terunuma, K. Oikawa, M. Shimizu, S. Sudo, K. Sagawa, Fluoride-based erbium-doped fiber amplifier with inherently flat gain spectrum, IEEE Photonics Technology Letters 8 (1996) 882–884.
[5] E. Downing, L. Hesselink, J. Ralston, R. Macfarlane, A Three-Color, Solid-state, three-dimensional display, Science 273 (1996) 1185–1189.
[6] Y. Wang, J. Ohwaki, New transparent vitro ceramics codoped with Er^{3+} and Yb^{3+} for efficient frequency upconversion, Applied Physics Letters 63 (1993) 3268–3270.
[7] M.J. Dejneka, The luminescence and structure of novel transparent oxyfluoride glass ceramics, Journal of Non-Crystalline Solids 239 (1998) 149–155.
[8] D. Chen, Y. Wang, E. Ma, Y. Yu, F. Liu, Partition, luminescence and energy transfer of Er^{3+}/Yb^{3+} ions in oxyfluoride glass ceramic containing CaF_2 nano-crystals, Optical Materials 29 (2007) 1693–1699.
[9] Z. Pan, A. Ueda, R. Mu, S.H. Morgan, Upconversion luminescence in Er^{3+}-doped germanate–oxyfluoride and tellurium–germanate–oxyfluoride transparent glass–ceramics, Journal of Luminescence 126 (2007) 251–256.
[10] I. Gugov, M. Muller, C. Russel, Transparent oxyfluoride glass ceramics co-doped with Er^{3+} and Yb^{3+}—crystallization and upconversion spectroscopy, Journal of Solid State Chemistry 184 (2011) 1001–1007.
[11] F. Zeng, G. Ren, X. Qiu, Q. Yang, J Chen, The effect of PbF_2 content on the microstructure and upconversion luminescence of Er^{3+}-doped SiO_2–PbF_2–PbO glass ceramics, Journal of Non-Crystalline Solids 354 (2008) 3428–3432.
[12] A.D. Pablos-Martın, N. Hémono, G.C. Mather, S. Bhattacharyya, T. Hoche, H. Bornhoft, J. Deubener, F. Munoz, A. Duran, M.J. Pascual, Crystallization kinetics of LaF3 nanocrystals in an oxyfluoride glass, Journal of the American Ceramic Society 94 (2011) 2420–2428.
[13] S. Ghosh, D. Divya, K.C. Remani, T.S. Sreeremya, Growth of monodisperse nanocrystals of cerium oxide during synthesis and annealing, Journal of Nanoparticle Research 12 (2010) 1905–1911.
[14] L.L. Kukkonen, I.M. Reaney, D. Furniss, M.G. Pellatt, A.B. Seddon, Nucleation and crystallization of transparent erbium III-doped, oxyfluoride glass ceramics, Journal of Non-Crystalline Solids 190 (2001) 25–31.
[15] M. Avrami, Kinetics of phase change. I. General theory, Journal of Chemical Physics 7 (1939) 1103–1112.
[16] M. Avrami, Kinetics of phase change. Ii. Transformation-time relations for random distribution of nuclei, Journal of Chemical Physics 8 (1940) 212–214.
[17] M. Avrami, Kinetics of phase change. III. Granulation, phase change and microstructure, Journal of Chemical Physics 9 (1941) 177–184.
[18] J. Alton, T.J. Plaisted, Kinetics of growth of spinel crystals in a borosilicate glass, Chemical Engineering Science 57 (2002) 2503–2509.
[19] O. Grong, O.R. Myhr, Additivity and isokinetic behaviour in relation to diffusion controlled growth, Acta Materialia 48 (2000) 445–452.
[20] J.W. Cahn, The kinetics of grain boundary nucleated reactions, Acta Metallurgica 4 (1956) 449–459.
[21] J.W. Cahn, Transformation kinetics during continuous cooling, Acta Metallurgica 4 (1956) 572–575.
[22] H.E. Kissinger, Variation of peak temperature with heating rates in differential thermal analysis, Journal of Research of the National Bureau of Standards 57 (1956) 217–221.
[23] H.E. Kissinger, Reactions kinetics in differential thermal analysis, Analytical Chemistry 29 (1957) 1702–1706.
[24] T. Ozawa, Kinetics of non-isothermal crystallization, Polymer 12 (1971) 150–158.
[25] T. Ozawa, Temperature control modes in thermal analysis, Pure and Applied Chemistry 72 (2000) 2083–2099.
[26] J.A. Augis, J.E. Bennett, Calculation of the Avrami parameters for heterogeneous solid state reactions using a modification of the Kissinger method, Journal of Thermal Analysis 13 (1978) 283–292.
[27] K. Cheng, Evaluation of crystallization kinetics of glasses by non-isothermal analysis, Journal of Materials Science 36 (2001) 1043–1048.
[28] Y.J. Park, J. Heo, Nucleation and crystallization kinetics of glasses derived from incinerator fly ash waste, Ceramics International 28 (2002) 669–672.
[29] L.A. Perez-Maqueda, J.M. Criado, J. Malek, Combined kinetic analysis for crystallization kinetics of non-crystalline solids, Journal of Non-Crystalline Solids 320 (2003) 84–91.
[30] K. Matusita, S. Saka, Kinetic-study on crystallization of glass by differential thermal-analysis criterion on application of Kissinger plot, Journal of Non-Crystalline Solids 39 (1980) 741–746.